STRUCTURE DEFECTS AND ELECTROCHEMICAL STUDY OF COPPER PROCESSED BY EQUAL CHANNEL ANGULAR PRESSING

Rakia DALY [a*], Mohamed MASMOUDI [b]

[a] *Unité de Recherche « Electrochimie et Environnement », Ecole Nationale d'Ingénieurs de Sfax, BPW 3038, Université de Sfax, Tunisie.*
[b] *Laboratoire de Chimie Inorganique, Faculté des Sciences de Sfax, Université de Sfax, BP 1171, Sfax 3018, Tunisie.*

(Reçu le 26 Juin 2013, accepté le 08 Février 2014)

ABSTRACT: Ultra-fine grained (UFG) pure copper of 99.99 wt.% purity has been successfully obtained at room temperature by Equal Channel Angular Pressing (ECAP), with the grain size about 200 nm after 2 passes. X-ray diffraction and Transmission Electron Microscopy (TEM) were used to characterize the microstructure evolution. The effect of ECAP passes on the electrochemical behavior of copper were investigated by potentiodynamic polarization test. The UFG copper display a higher corrosion resistance, despite the increase of the defect density, such as dislocations and grain boundaries.

Keywords: ECAP, X-ray diffraction profile analysis, TEM, potentiodynamic polarization, Corrosion.

1. Introduction

Nanocrystalline and submicrocrystalline materials stimulated recently considerable interest among researchers [1]. These materials are characterized by a very fine grain size and a large amount of grain boundary area. The presence of a large amount of grain boundary area results in unusual and extraordinary changes in both mechanical and physical properties.

Recent investigations have shown that sever plastic deformation (SPD) is an effective method for forming submicron-grained material [2-4]. One of the most common SPD methods is the Equal Channel Angular Pressing (ECAP) [5]. This technique has an important benefit; in fact, very high plastic strains can be attained in relatively thick-sectioned products. This significant advantage has resulted in ECAP, is emerging as an important metal processing method for obtaining extremely fine grain structures in alloys in bulk forms. While the strength increases spectacularly after ECAP, the ductility remains relatively high or even increases in some cases.

The influence of corrosive environment on service characteristics such as resistance to corrosion of ultra-fine grain (UFG) materials fabricated by SPD is a practically important issue which has received attention for the last 10 years [6-9].

Recently, there are a number of reports dealing with the microstructure of aluminum and its alloys processed by ECAP [10-14], in which submicron sized grains with sharp boundaries were formed. In addition to aluminum and its alloys , copper is another typical FCC metal for model studies, which has relatively lower stacking fault energy (SEF) such that dislocation cross-slip is expected more difficult in it. However, the reports on the microstructure of copper deformed by ECAP are relatively scarce [15].

The present work focused on the influence of microstructure change on the corrosion behavior of pure copper processed by ECAP. Electrochemical investigations on the as-received and ECAP copper were performed in 3% NaCl aqueous solution, complemented by microstructural study. The results should be helpful for better understanding the corrosion behaviour of ECAP copper, and exploiting their possible engineering application.

* Corresponding author e-mail: daly.rakia@gmx.fr

2. Materials and experimental methods

2.1. Samples and severe plastic deformation process

The starting material for the experiments was OFHC copper (99.99% purity) annealed for 24 h at 600°C under a low pressure of purified argon to ensure homogeneous structure before pressing, and quenched in iced water. Processed samples were with a dimension of 10 x 10 x 70 mm^3. The ECAP process consists in forcing a specimen to pass through two channels of equal cross-section interesting at an angle. After passing through the channels, the sample, while retaining its original geometry, has undergone a shear deformation which under typical conditions (Φ= 90°, i.e. perpendicular channel). The ECAP-die was shown in Fig. 1. Three orthogonal planes X, Y and Z with the associated directions were defined. In this work, only tow pressings of the sample without rotation between two successive passes (route A) are prepared. The ECAP was carried out at room temperature with MoS_2 as lubricant.

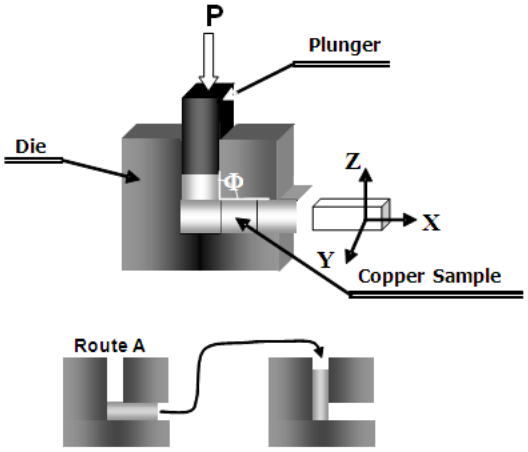

Figure. 1 : Schematic illustration of ECAP technique.

2.2. Structural and morphological characterizations

X-ray diffraction was performed on a wide angle diffractometer in the θ-2θ step scan mode by using Cu-Kα radiation. Scans were collected over a 2θ range of 30-120° with a step of 0.02°. A 10 s acquisition time was used at each step to obtain good statistics. The crystallite size and the equivalent lattice strain were determined from the Full Width Half Maximum (FWHM), β, of reflections using the Halder - wagner approach [16]. The peaks shapes were approximated by the $K_{\alpha 1}$ + $K_{\alpha 2}$ superposition of Voigt functions by using a WinPLOTOR software. The lattice parameters of the sample before and after ECAP were obtained from a linear regression analysis of the measured lattice parameter, obtained from each peak, plotted against the Nilson-Reley function [17]. The error bars were obtained by calculation of the standard deviation on the lattice parameter values calculated from each peak. We have concluded that the resulting error of the lattice parameter value does not exceed 0.025%.

To evaluate morphological evolution of samples after ECAP used in the present investigation were studied by using the Transmission Electron Microscopy (TEM) JEOL 2000 EX at acceleration voltage of 200 KV.

2.3. Potentiodynamic polarization tests

The potentiodynamic polarization curves of the copper were accomplished with a Radiometer's Electronic Potentiostat Galvanostat controlled by the software VoltaLab. The potentiostat was programmed to apply a continuously varying potential to the sample at a rate of 0.2 mV/s. All potentials were measured against the saturated calomel electrode (SCE), and a graphite electrode was used as the counter electrode. The specimen was finished by grinding with 1200-grit silicon carbide (SiC) paper. All experiments were performed in aerated NaCl 3% solution, at room temperature. For each material and electrolyte combination, the corrosion sample was allowed to be stabilized in electrolyte for 40 min. To ensure the reproducibility, at least three replicates were run for each specimen.

3. Results and discussion

3.1. Microstructure after ECAP

Fig. 2a shows typical X-ray diffraction patterns taken on the X-plane of the samples before and after ECAP. It contains the (111), (200), (220), (311) and (222) reflections of the Cu phase. A slight {111}-texture exists in the different samples according to the relative maximum intensity of each Bragg reflection peaks. Moreover, it can be seen, line broadening increases with ECAP. This broadening is related to the changes of microstructure, i.e., the reduction of crystallite size and lattice strain introduced by using a process of plastic deformation by ECAP. Fig. 2b shows typical X-ray (200)-peak broadening before and after ECAP; the progressive broadening of the (200)-peak with ECAP is clearly observed.

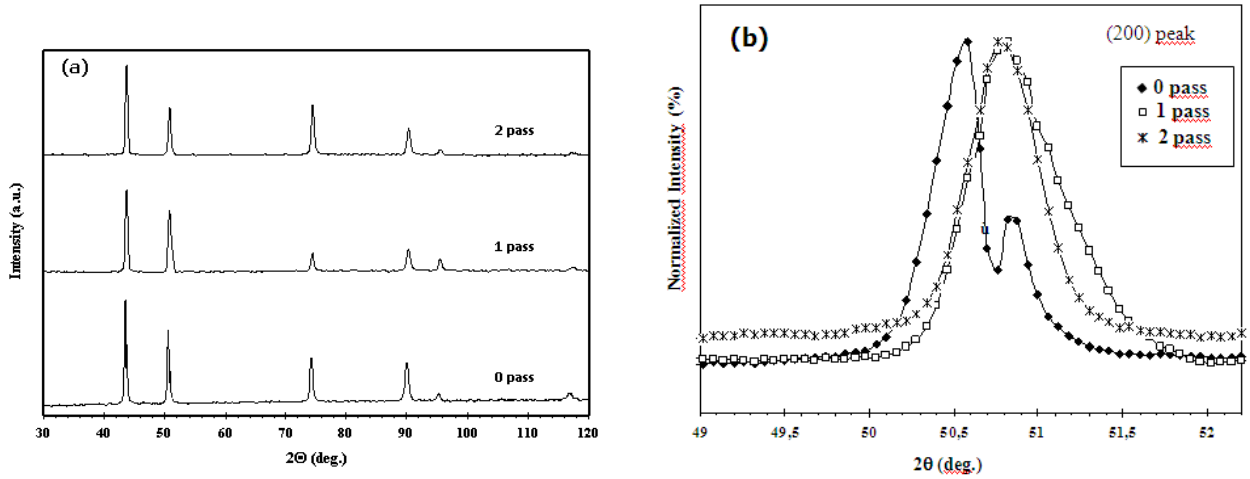

Figure 2 : (a) : Typical X-ray diffraction patterns taken on of the samples before and after ECAP. ,(b) : The (2 0 0) peak recorded in the X-plane before and after ECAP.

The lattice strain and the crystallites sizes calculated using the Halder – Wagner method [16], are given in table. 1, they reach 0.33% for the lattice strain, whereas the crystallite size achieved after 1 and 2 passes are about 280 nm and 220 nm respectively.

Table I : The lattice strain and the crystallites sizes calculated evolution during ECAP processing.

	0 pass	1 pass	2 passes
Microstrains (%)	-	0.33	0.56
Crystallites size	40 μm	280 nm	220 nm

The grain refinement, after ECAP, is clearly achieved with high level of strain. This behavior should be related to an important plastic deformation occurs during pressing in the die which increases the lattice strain because of the increase of the defect density, i.e. dislocations, grain boundaries, lattice defects with their characteristic strain fields.

From a direct examination of diffraction patterns before and after ECAP, we note, in the deformed samples, that peaks are slightly shifted to high θ values. It is not easy to draw a clear conclusion about this effect since many features should operate simultaneously: the creation of stacking faults by severe plastic deformation is probably one of the reasons of this shift. Another feature is the decrease of lattice parameter: which should arise from a compression of the lattice due to an ultrafine-grains structure obtained mainly for the deformed samples. We have calculated the lattice parameter values before and after ECAP by using the Nilson-Reley function. The obtained

values are presented in table. 2. We note that the lattice parameter decreases after pressing and reach a value of 3.6275 Å after one pass.

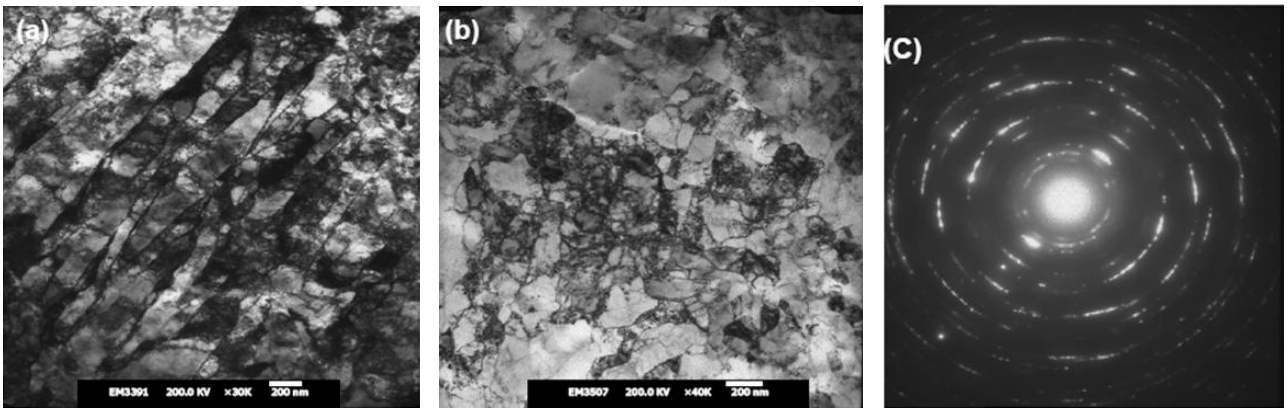

Figure 3: Microstructure of copper prepared by ECAP (1 pass): (a) and (b) TEM micrographs of the microstructure in two magnifications, (c) selected area diffraction patterns

Table II The lattice parameter values before and after ECAP.

	0 pass		1 pass		2 passes	
Peak	*FWHM*	*a (Å)*	*FWHM*	*a (Å)*	*FWHM*	*a (Å)*
(111)	0.317		0.458		0.404	
(200)	0.303	3.6368	0.633	3.6275	0.446	3.6288
(220)	0.471		0.492		0.472	
(311)	0.597		0.584		0.560	
(222)	0.443		0.519		0.524	

Fig. 3a and 3b represents the typical bright-field TEM images showing the microstructures of the investigated samples observed in the X planes after the single pass through the die. Some areas with banded type structure were clearly observed (Fig. 3a). These bands appear fragmented into smaller grains with a width of ≈200 nm (Fig. 3b). The boundaries between the bands appear straight and well defined; the dislocation density inside the bands is rather high. Fig. 3c shows the corresponding electron diffraction patterns (SADP), we note that diffraction spots are still resolved even through they are slightly elongated; this indicated a low misorientations between the newly created grains accompanied by an eventual distortion of the lattice. Although the grain sizes estimated from TEM analysis (≈200 nm) differ slightly from those calculated from the XRD analysis (≈260 nm), this small difference is due to that MET is a direct measurement technique while the DRX is based on mathematical equations. The investigated microstructure should be formed during severe plastic deformation, since no subsequent heating was carried out. Its characteristic features are the existence of high internal stresses which is confirmed by the bending extinction contours observed inside the grain boundary and the presence of extrinsic grain boundary defects.

Fig. 4 presents typical images showing the very high dislocation density within the grains copper after 2 passes. Fig. 4a shows rather thick regions of the foil sample where many fringes are observed, leading to the description of the deformed state as one that has non-equilibrium boundaries, with indeterminate, fuzzy contrast [18, 19]. In other area of the same sample some arrangement of the dislocations into cell and sub-grain boundaries are also observed in Fig. 4b.

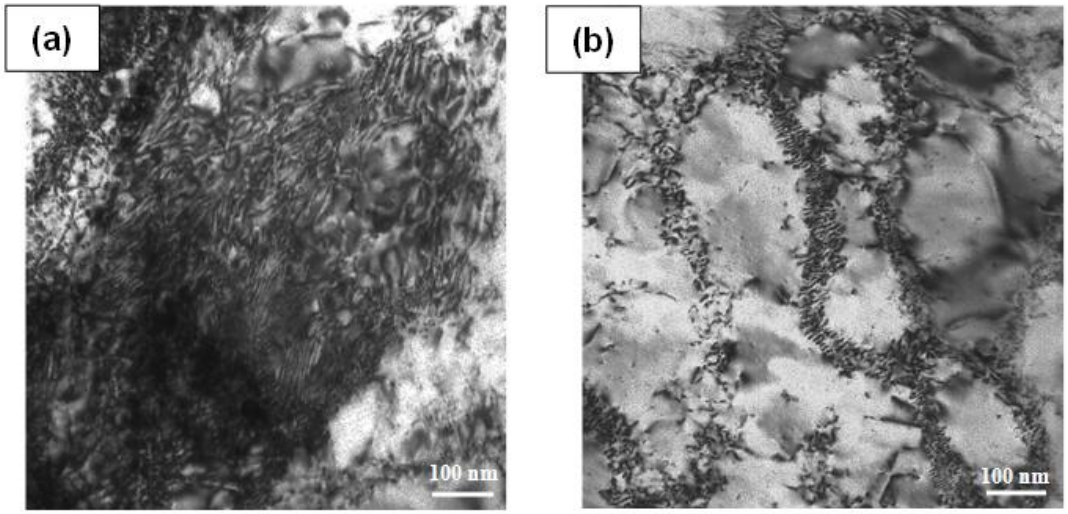

Figure 4: TEM images showing (a) fuzzy boundary fringe patterns and (b) dislocation rearrangement as cell and sub grain boundaries in the copper after 2 passes.

3.2. Electrochemical investigation.

The potentiodynamic polarization curves of the copper electrode in aerated NaCl 3% solution after (a) 0 pass, (b) 1 pass and (c) 2 passes are shown in Fig. 5.

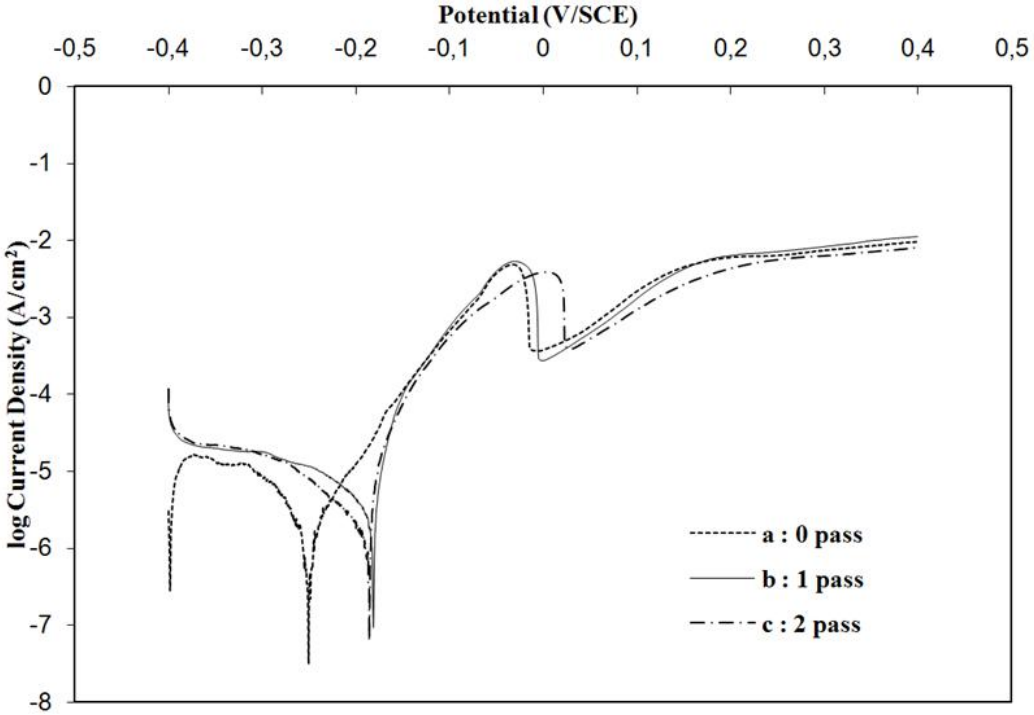

Figure 5 : Potentiodynamic polarization curves for ECAP processed copper in NaCl 3% solution.

The cathodic reaction of copper in aerated sodium chloride solutions is well known to be the oxygen reduction [20],

$$O_2 + 2H_2O + 4e^- \rightarrow 4OH^- \quad (1)$$

The equal channel angular pressing 1 and 2 passes, slightly increases the cathodic current and to some extent the anodic current.

The proposed mechanism for copper anodic dissolution in chloride media is divided to three stages as shown in the scheme presented in Fig. 6 [21-23].

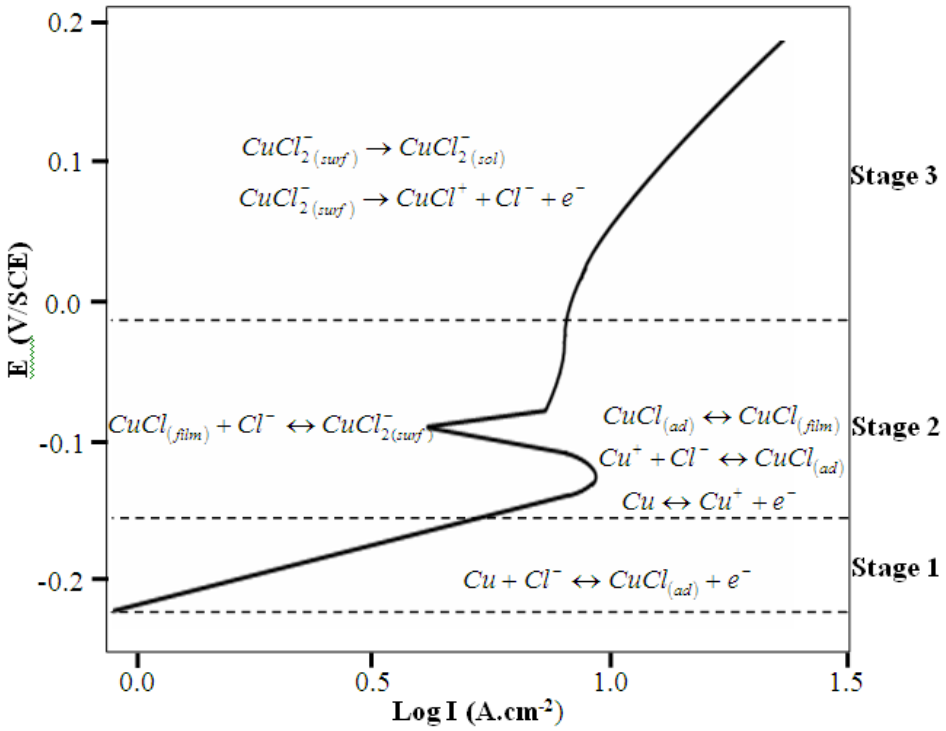

Figure 6 : Typical anodic polarization characteristics of copper in aqueous chloride media.

Stage 1. The initial reaction is between chloride ions and copper metal in the solution resulting in the formation of *CuCl* layer, which is the least soluble of the copper chlorides on the anodic as described by the Eq. (2) [24].

$$Cu + Cl^- \leftrightarrow CuCl_{ads} + e^- \qquad (2)$$

In this stage, a potential region of "apparent Tafel" behavior is observed. Both charge transfer and mass transport controlling kinetics are usually assumed. As indicated in Fig. 5, the slope of this stage for copper 0 pass is different from the copper after 1 and 2 passes, which is related to difference in kinetics parameters before and after ECAP.

Stage 2. The depletion of chloride ions will yield a rather well-defined electrode potential which corresponds to a copper electrode in a *CuCl* saturated solution with in the absence of excess electrolyte, especially *NaCl* . When the surface is covered, the anodic dissolution of copper occurs through oxidation of metallic copper to cuprous ion, which can be shown as Eq. (3) [25-26].

$$Cu \rightarrow Cu^+ + e^- \qquad (3)$$

This in turn reacts with chloride ion from the solution to form CuCl film:

$$Cu^+ + Cl^- \rightarrow CuCl_{ads} \qquad (4)$$

$$CuCl_{ads} \rightarrow CuCl_{(film)} \qquad (5)$$

The equilibrium potential of Eq. (4) is described as function of chloride ion in Eq. (6) [27].

$$E_{equi} = -0.105 - 0.059 \log [Cl^-] (V_{SCE}) \qquad (6)$$

For the chloride concentration in this study, the E_{equi} obtained about - 0.088 V versus SCE. As shown in potentiodynamic polarization curves (fig. 5), the first peak for all samples is attributed to

both Eq. (4) and (5).

Mass transport controls the kinetic of the potential range where limiting the current density. Under this condition, the adsorbed $CuCl$ layer has poor adhesion, does not provide enough protection for copper, and transforms to the soluble copper chloride complex, $CuCl_2^-$ [28].

$$CuCl_{2(film)} + Cl^- \rightarrow CuCl^-_{2(surface)} \quad (7)$$

Before ECAP the potential region between -6 and 27 mV versus SCE is attributed to passivation zone. After ECAP passes this region shifted towards positive potentials especially after 2 passes (21 – 38) mV versus SCE. Furthermore, we noted a slightly increases of both passivation current density (I_p) and passivation potential (E_p). The corrosion potential (E_{corr}) increases from -248 mV versus SCE for Cu 0 pass to -183 mV and -181 mV versus SCE after 1 and 2 passes respectively. As can be seen from table.3, the positive shift of around 65 mV versus SCE in E_{corr} and the slightly increases in corrosion current density (J_{corr}) indicate the relatively better corrosion behavior of copper after ECAP passes, despite the fact that this result is totally unexpected for copper according to prior research [8,29]. Indeed, ECAP copper increases the defect density, such as dislocations and grain boundaries.

Table III : Parameters obtained from potentiodynamic polarization curves.

	0 pass	1 pass	2 passes
E_{corr} (mV/SCE)	-248	-183	-181
J_{corr} ($\mu A/cm^2$)	5.2	3.2	2.4

Stage 3. At higher potential, any increase in current density is due to the electrodissolution of copper and the diffusion of soluble $CuCl_2^-$ from Helmoltz plan in the bulk solution [30]. Also in this stage the kinetics are controlled by both charge transfer and mass transport. Eq. (8) and (9) show this stage:

$$CuCl^-_{2(surface)} \rightarrow CuCl^-_{2(solution)} \quad (8)$$

$$CuCl^-_{2(surface)} \rightarrow Cu^{2+} + 2Cl^- + e^- \quad (9)$$

Reasonably, in chloride containing medium, Cl^- usually takes part in the whole process of copper corrosion, including surface adsorption, chelation, and film formation. Furthermore, Cl^- also plays a vital role in acceleration of copper corrosion [31]. The corrosion products from reactions (3)-(5) are porous $CuCl$ which can react with water and form Cu_2O (Eq (10)) in succession. Then the surface of copper electrode is covered with an insoluble compound layer containing $CuCl$ and Cu_2O [32]. The Cl^- in the environment can easily penetrate into the porous film, and accelerate the corrosion of copper substrate.

$$2CuCl_{(film)} + H_2O \rightarrow Cu_2O + 2H^+ + 2Cl^- \quad (10)$$

4. Conclusions

Severe plastic deformation under ECAP, allowed copper to be highly deformed with a mainly granular ultrafine structure, about 200 nm in size. In this deformed state, compound has high level of lattice strains, this affects the electrochemical properties apart through potentiodynamic polarization tests that revealed a slightly high corrosion resistance of the ECAP copper specimens tested in NaCl 3% solution especially after 2 passes.

References

[1] C. Suryanarayana, D. Mukhopadhyay, S. N. Patankar, and F. H. Froes, J. Mater. Res., 7(1992), 2114.
[2] R. S. Musalimov and R. Z. Valiev, Scripta Metall. Mater., 27(1992), 1685.
[3] R. Z. valiev, A. V. Korznikov, R. R. Mulyukov. Mater. Sci. Eng., A168 (1993) 141-148.
[4] J. Languillaume, F. Chmelik, G. Kapelski, F. bordeaux, A.A. Nazarov, G. Canova, C .Esling, R. Z. Valiev, and B. Baudelet, Acta Metall. Mater., 41 (1993), 2953.
[5] V.M. Segal, V.I. Reznikov, A.E. Drobyshevskiy, V.I. Kopylov, Russian Metall 1 (1981) 99.
[6] A. Vinogradov, T. Mimaki, S. Hashimoto, R.Z. Valiev, Scripta Mater. 41 (1999) 319–326.
[7] A. Vinogradov, H. Miyamoto, T. Mimaki, S. Hashimoto, Ann. Chim. Sci. Mat. 27 (2002) 65–75.
[8] T. Yamasaki, H. Miyamoto, T. Mimaki, A. Vinogradov, S. Hashimoto, Mater. Sci. Eng. A 318 (2001) 122–128.
[9] H. Miyamoto, T. Mimaki, A. Vinogradov, S. Hashimoto, Ann. Chim. Sci. Mat. 27 (2002) S197–S206
[10] M. Kawazoe, T. Shibata, T. Shibata, T. Mukal, and N. A. Krasilnikov, J. Mater. Sci. Let., 9 (1990).
[11] M. Markusev, C. C. Bampton, M. Y. Murashkin, and D. A. Hardwick, Mater. Sci. Eng., A234-236 (1997), 927.
[12] N. K. Tsenev, R. Z. Valiev, and I. R. Kuzeev, Mater. Sci. Forum, 242 (1997), 127.
[13] S. Komura, P. B. Berbon, M. Furukawa, Z. Horita, M. Nemota, and T. G. Langdon, Scripta Metall. Mater., 38 (1998), 1851.
[14] T. Mukai, M. Kawazoe, and K. Higashi, Mater. Sci. Eng., A247 (1998), 270.
[15] R.Z. Valiev, E. V. Kozlov, Y. F. Ivanov, J. Lian, A. A. Nazarov, and B. Baudelet, , Acta Metall. Mater., 42 (1994), 2467.
[16] J.I. Langford, National Institue of Standards and technology Special publication 846, in: Proceedings of the International conference Accuracy in powder Diffraction II, NIST, Gaithersburg, MD, 1992.
[17] L.V. Azaroff, M. Buerger, The Powder Method, McGrow Hill, New York,
[18] R.Z. Valiev, NanoStruct Mater 6 (1995) 73.
[19] Wang J, Iwahashi Y, Horita Z, Furukawa M, Nemoto M,
[20] E.M. Sherif, R.M. Erasmus, J.D. Comins. J. Appl. Surf. Sci. 252 (2006) 8615.
[21] G. Kear, B.D. Barker, F.C. Walsh, Corros. Sci. 46 (2004) 109.
[22] E.M. Sherif, R.M. Erasmus, J.D. Comins, J. Colloid Interface Sci. 311 (2007) 144.
[23] H.-B. Lu, Y. Li, F.-H. Wang, Corros. Sci. 48 (2006) 2106.
[24] M. Saremi, M. Yeganeh; Materials Chemistry and Physics 123 (2010) 456–462.
[25] J. L Wang, C.C Xu, G.C Lv,. Applied Surface Science, 2006, 252 (18): 6294.
[26] H Strandberg, Atmosperic Environment, 1998, 32 (20): 3521
[27] H.P. Lee, K. Nobe, J. Electrochem. Soc. 132 (1985) 1031.
[28] E.M. Sherif, R.M. Erasmus, J.D. Comins, J. Colloid Interface Sci. 306 (2007) 96
[29] H. Miyamoto, K. Harada, T. Mimaki, A. Vinogradov, S. Hashimoto, corro. Sci. 50 (2008) 1215–1220.
[30] L. Bacarella, J.C. Griess, J. Electrochem. Soc. 120 (1973) 459.
[31] G.Horanyi, E.M. Rizmayer, P.J. Joo, Electroanal. Chem.,1983, 149 : 221.
[32] A.V. Benedetti, P.T.A. Sumodjo, K. Nobe, P.L. Cabot, W.G. Proud, Electrochimica Acta, 1995, 40: 2657 16.